Impact of a water restriction on the summer climatic benefits of trees inside an outdoor street canyon scale model

J. Thierry, S. Herpin, R. Levi, D. Canonne, S. Demotes-Mainard, Patrice Cannavo, D. Lemesle, F. Rodriguez, P.E. Bournet

Building and Environment 261 (2024) 111722

Contents lists available at ScienceDirect

Building and Environment

journal homepage: www.elsevier.com/locate/buildenv

Impact of a water restriction on the summer climatic benefits of trees inside an outdoor street canyon scale model

J. Thierry [a,b,c,f], S. Herpin [a,b,c,*], R. Levi [a,b,c], D. Canonne [a,b,c,d], S. Demotes-Mainard [c,d], P. Cannavo [a,b,c], D. Lemesle [a,b,c], L. Brialix [a,b,c], F. Rodriguez [b,e], P.E. Bournet [a,b,c]

[a] Institut Agro, EPHor, 49000, Angers, France
[b] IRSTV, FR CNRS 2488, 44321, Nantes Cedex 3, France
[c] QuaSaV, SFR 4207, 49000, Angers, France
[d] Univ Angers, Institut Agro, INRAE, IRHS, 49000, Angers, France
[e] Université Gustave Eiffel, GERS-LEE, 44344, Bouguenais, France
[f] Ville de Paris, DEVE, STVA, DESV, 75012, Paris, France

ARTICLE INFO

Keywords:
Radiation interception
Water balance
Transpiration
Human thermal comfort
UTCI
Urban environment

ABSTRACT

Trees may help reduce the increasing human thermal stress in cities caused by the Urban Heat Island phenomenon and the multiplication and intensification of heatwaves through the climatic benefits they provide: cast shadows and transpiration. However, the multiplication of droughts may lower the water supply of street trees and impact their development and climatic benefits. The transpiration and radiation interception of two alignments of potted ornamental apple trees (*Malus Coccinella*® 'Courtarou') planted in a 1/5 scale street canyon experiencing contrasted water supplies were monitored during an 8-week period of summer 2022. Compared to well-watered trees, the transpiration of water-restricted trees was reduced quickly and strongly by 81 % on average. A noticeable reduction of the leaf area index of the water-restricted trees led to a decrease of their radiation interception which however remained higher than 69 % of the incident radiation measured without trees. No noticeable air temperature difference was measured under the tree crowns of both alignments of trees but the Universal Thermal Climate Index calculated under the water-restricted trees increased by on average 1 °C. Radiation interception appeared to be responsible for the major part of the daily total amount of energy dissipated. A noticeable reduction of the daily total amount of energy dissipated by the WR trees was mostly attributed to the reduction of their transpiration which may explain why both alignments of trees kept providing noticeable climatic benefits.

1. Introduction

The multiplication and intensification of extreme climatic events such as heatwaves accompanying climate change is observed in all regions of the world [1]. In France, the average annual duration of heatwaves was 1.7 days.year^{-1} before 1989 whereas it reached 7.95 days.year^{-1} since 2000 [2]. In cities, heatwaves add to a pre-existing overheating phenomenon called Urban Heat Island (UHI) [3–5] which is influenced by multiple factors such as the nature of the materials or the urban geometry [6,7]. Thereby, the combination of heatwaves and UHI exposes the city dwellers to a thermal stress which may cause sanitary issues [1,8]. In France, around 15 000 deaths were attributed to the heatwave of summer 2003 and the mortality risk appeared to be higher in cities where the UHI intensifies the overheating especially at night [9].

In order to mitigate urban overheating and thereby human thermal stress, multiple works assessed the climatic benefits of vegetation which mainly come from two main processes: cast shadow and transpiration. The cast shadow reduces the amount of solar radiation reaching the surrounding surfaces whereas the water transpired by the trees takes off energy of the surrounding atmosphere to evaporate. Vegetation can be implemented in cities through different configurations such as green facades [10,11], green roofs [12,13], grass covers, urban parks [14,15] or street trees [16,17]. Yet, street trees appear to be particularly interesting for both overheating and human thermal stress mitigation as they can cast shadows on buildings, on the ground and on the pedestrians.

The impact of individual trees on urban microclimate was

* Corresponding author. Institut Agro Rennes-Angers, Campus d'Angers, 2 rue André Le Nôtre, 49045, Angers Cedex 01, France.
E-mail address: sophie.herpin@institut-agro.fr (S. Herpin).

https://doi.org/10.1016/j.buildenv.2024.111722
Received 26 November 2023; Received in revised form 31 May 2024; Accepted 4 June 2024
Available online 8 June 2024

Abbreviations

A.g.l	above ground level
LAI	leaf area index
NR-AWS	non-readily available water storage
PAR	photosynthetically active radiation
R-AWS	readily available water storage
TAWS	total available water storage
UHI	Urban Heat Island
VWC	volumetric water content
WR	water-restricted
WW	well-watered

highlighted through the quantification of the incident solar radiation they intercept [18,19], the temperature reduction of the surrounding surfaces [20,21], the reduction of globe temperature [22] and mean radiant temperature [23] under their crowns. Some works quantified the energy dissipated through the evaporation of the water they transpire [24,25] and a variety of diurnal air temperature reductions were reported [26,27]. Human thermal stress was approached by a variety of indicators aiming at taking the complete thermal balance of a human body into account. Among them, the Universal Thermal Climate Index (UTCI) [28] is widely used in the literature for the assessment of outdoor thermal environment because it relies on a highly detailed human body model [29]. Thereby, a variety of UTCI reductions beneath the tree canopy compared to reference open areas can also be found in the literature [30,31]. Multiple works focused on street canyons, a common urban configuration, which appeared to be adapted to study urban overheating at street scale [32,33] and its impact on the pedestrians. Other works relied on the use of reduced scale models which are more convenient to perform continual monitoring and allow to control more parameters such as building heights and surface materials [34,35,]. Mballo et al. [36], for instance, estimated that cast shadows were responsible for 74 % of the cooling benefits of well-watered trees during a single sunny day inside a 1/5 scale north-south oriented street canyon whereas the remaining 26 % were attributed to the evaporation of the transpired water. For a large panel of weather conditions and considering 120 studied days, Herpin et al. [37] extended their work and calculated an average air temperature reduction of 2 °C and an average UTCI reduction of 5.3 °C under the studied well-watered trees compared to a non-vegetated zone of the street canyon.

However, the health and development of street trees rely on a sufficient access to water into the soil. Yet, the intensity, frequency and distribution of rainfalls are expected to be locally modified due to the ongoing climate change [1] and the water resources of trees will not be guaranteed all along the growing season in the near future. Schütt et al. [38] monitored the soil water potential inside the tree pits of 17 street trees in 2018–2019 and revealed that street trees were already experiencing critical soil water potential during three to five months per year.

When exposed to a decreasing soil water potential, trees try to avoid cavitation and embolism by adjusting their stem water potential especially by closing their stomata or reducing their leaf area [39,40], two mechanisms that may alter their gas exchanges and light interception, and by the way, their photosynthetic activity and transpiration. The response time of these mechanisms may vary a lot [41]. The stomatal closure can be noticed from one day to the next one [42] whereas morphological adjustments may take several weeks. Thus, the ability of street trees to maintain significant climatic benefits under such conditions needs to be studied as it is a major concern for urban planners who need to understand how nature-based solutions may help reduce human thermal stress in cities in a context of rarefying water resources. Yet, it appears that few works studying the climatic benefits of street trees carried out continuous monitoring [20,43] enabling to assess the effect of dry periods, and none of them could so far control or monitor soil water availability.

Some studies assessed the seasonal changes of tree transpiration or related variables with a varying soil moisture [44]. Others, highlighted significant reductions of transpiration ranging from 25 % [45] to 92 % [46] when comparing well-watered and water-restricted trees of various species. Gebauer et al. [47] and Konarska et al. [48] observed a significant decrease of stomatal conductance (i.e. stomatal closure) during dry periods. Dervishi et al. [49] found lower morphological variables such as leaf area density for young potted water-restricted *Platanus x hispanica* and *Tilia cordata* compared to well-watered ones. However, the studies controlling or monitoring soil water availability were not meant to study climatic benefits or only assessed part of the variables related to the tree cooling potential. A preliminary work of Thierry et al. [50] evaluated the effect of a 1-week water restriction on street trees climatic benefits but no impact on the tree foliage was reported as the water shortage was too short and moderate.

Thus, the objective of the present study is to understand and quantify the influence of a long water restriction period on the climatic benefits provided by street trees and the processes they rely on. It proposes an original assessment of the effect of the lack of water on both tree transpiration and shadows cast by the trees and analyses the evolution of their respective contributions to the climatic benefits over time. To achieve these goals, an original integrated approach of the soil-plant-atmosphere continuum is proposed including the continuous monitoring of the water availability in the soil, tree transpiration and radiation interception, and the surrounding microclimate inside a reduced scale street canyon vegetated with both water-restricted and well-watered trees during a 2-month summer period.

2. Materials and methods

2.1. Materials

The present study was run over July and August 2022. The air temperature of the studied period was on average 2 °C higher than the reference average climatic conditions recorded at the Météo-France meteorological station (see section 2.1.3, reference period: 1991–2020) whereas the total rainfall was twice lower. The two studied months were characterized by an alternation of warm, sunny and rain-free periods (especially the two first weeks of July and August) characterized by a high reference evapotranspiration and insolation ratio, and of cloudy and rainy periods (from July 19th to 22nd and from August 13th to 26th) which lowered both the reference evapotranspiration and the insolation ratio (Figure B1 in appendix B).

2.1.1. General presentation of the street

The experiments were run in a 1/5 scale street canyon model located in Angers, France (47°28′47″ N, 0°36′33″ W). Angers is characterized by a Cfb temperate oceanic climate according to the Köppen-Geiger classification [51]. The street (Fig. 1) is oriented North-South, i.e. perpendicular to the direction of the prevailing winds which mainly come from the west, in order to limit the eventual wind-driven air flow exchanges between the different zones of the street. The street is bordered by two buildings made of 0.1 *m* thick white concrete walls insulated with 0.12 *m* thick expanded polystyrene on the inside. Wooden frames covered with steel panels were used to build the roofs and external walls of the buildings. The ground of the street is covered with a 0.04 *m* thick layer of asphalt. Given that both buildings are 2 *m* high and that the street is 2 *m* wide, it forms an urban canyon which aspect ratio is 1 (height of the buildings divided by the width of the street). The street is divided into three zones: one treeless zone in the southern part of the street and two treed zones in the northern part and middle of the street. Both treed zones contain 5 ornamental apple trees (*Malus Coccinella*® 'Courtarou') aligned on the North-South central axis of the street. In each zone, the three central trees were studied and the two border trees were used as

Fig. 1. South view picture of the street canyon (left) and south view picture of the WR zone (right).

buffer zones preventing eventual interactions between the three central trees of each zone and the other surrounding zones. The trees were 4 years old at the time of the experiment, all issued from cutting and grown in the same nursery (André Briant Jeunes Plants). They were planted in the street canyon on January 19th, 2022 and subjected to a winter structural pruning. Their upper and lateral axes were trimmed on June 23rd, 2022 so they could fit in the dimensions of the reduced street canyon. For the purpose of this study, the three zones will be referred as:

- The well-watered zone or WW zone for the vegetated zone located in the northern part of the street as it was fully irrigated all year long;
- The water-restricted zone or WR zone for the vegetated zone located in the centre of the street as it was subjected to a water restriction during 8 weeks;
- The non-vegetated zone or NV zone for the southern part of the street which does not contain any tree.

2.1.2. Soil compartment

Each tree was planted in an 80 L container placed below the street ground surface inside a pit dug along the central North-South axis of the street canyon (Fig. 2). The containers were filled with 46.3 L of a topsoil-compost mixture in a 60/40 % volume ratio (from now on referred as "soil") placed on top of a layer of stones and a layer of concrete with a slight slope aiming at facilitating drainage, all layers being separated from each other by geotextile. The 46.3 L volume of top-soil-compost mixture corresponds to a 5.8 m^3 volume of top-soil-compost at full scale when applying a geometrical reduction factor of $(1/5)^3$ and to an 8.9 m^3 volume for the entire pit considering that tree pits are generally filled with a 65/35 % volume ratio of topsoil-compost mixture and rocks which is very consistent with the planting conditions in cities as trees are generally planted in 10 m^3 pits [52]. The 60/40 % volume ratio used for the topsoil-compost mixture was chosen on the basis of the common practices of urban greening and on studies showing that a 40 % volume ratio of compost could ensure both good agronomic quality of the soil and tree growth at the long-term scale [53,54]. The texture of the topsoil-compost mixture was measured in the laboratory using granulometry analysis after decarbonisation according to the French standard NF *X*31-107: the topsoil contains 6.6 % (mass ratio) of clay, 30.1 % of silt and 63.3 % of sand and its texture can be classified as loamy-sand regarding the French GEPPA classification and sandy loam regarding the

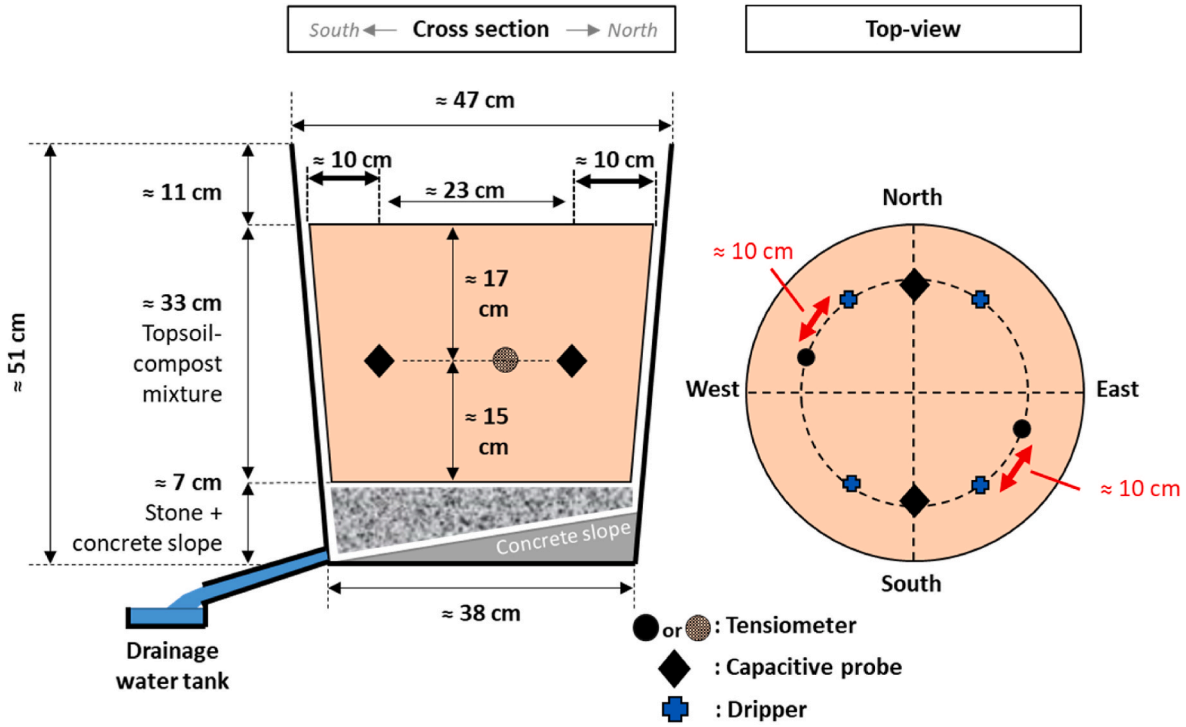

Fig. 2. Sketch of one of the three central planting containers of the vegetated zones and location of the sensors.

United States Department of Agriculture classification [55]. The topsoil-compost mixture contains 8.9 % (mass ratio) of organic matter.

The containers were covered with lids, and the pits with asphalt sheets preventing rainfall infiltration and direct evaporation from the soil. The trees were drip-irrigated daily between 20:00 and 22:00 UTC with fertilized water. The daily irrigation dose was chosen in order to maintain the soil moisture at field capacity and ensure well-watered conditions. The occasional drainage water was collected in a tank placed below every container and its volume was measured manually every working day (5 days/week).

The 3 central containers of each treed zone were equipped with 2 tensiometers and 2 capacitive probes each, all placed approximately at mid-depth of the topsoil-compost mixture, aiming at monitoring the water matric potential and the soil Volumetric Water Content (VWC) (Fig. 2).

The amount of water in the soil that a tree is able to collect is called the Total Available Water Storage (TAWS) and is defined by two soil VWC limits called field capacity and permanent wilting point. The field capacity is related to the texture of the soil and is generally associated to a water matric potential of approximately −0.033 MPa [56,57]. An experimental water retention curve, relating soil VWC and water matric potential, was established in the laboratory according to the French standard NF EN 13041 for the present topsoil-compost mixture and used to estimate the soil VWC associated to field capacity to 28 %. The permanent wilting point, depends on the soil texture but may also strongly rely on the considered plant. In the present experiment, the in-situ continuous monitoring of the soil VWC showed that when all water inputs and outputs were null except the water debited by the trees, soil VWC could not decrease under 10 %. This lower limit was then assumed to correspond to the permanent wilting point (see Fig. 6 presented and described later). The TAWS was then estimated to 18 % of the soil volume i.e. 8.3 L when considering the present soil volume of 46.3 L. Then, the TAWS is generally divided into a Readily AWS (R-AWS), where the plant is supposed to experience a comfortable access to water, and a Non-Readily AWS (NR-AWS) where pumping water may be more difficult for the plant which is likely to experience hydric stress. According to FAO et al. [58], the threshold delimiting the R-AWS and the NR-AWS should be located approximately at half of the TAWS for apple trees which means at a soil VWC of approximately 19 % for the present experiment.

2.1.3. Meteorological sensors

Although the French meteorological institute (Météo-France) operates a weather station called “Angers-Beaucouzé” (station n°49020001) located approximately 400 *m* away from the studied site, from now on referred as “Météo-France meteorological station”, on-site reference measurements were carried out with two meteorological masts located outside the street. The first one was aligned with the central North-South axis of the street and located 6.5 *m* north from the street (Figs. 1 and 3). The second one was located approximately 8 *m* west from the street (Fig. 1).

A set of meteorological sensors described in Fig. 3 was mounted in the central cross-section of each zone of the street in order to be representative of the microclimate of each zone and to avoid the sensors being influenced by the surrounding zones of the street. Especially, the respective location of the two vegetated zones ensured that the shadow cast by WR trees could only reach the southernmost WW tree, which was a not studied border tree, but not the meteorological sensors of the WW zone. The sensors were mounted at different heights above ground level (a.g.l.) including 0.4 *m* a.g.l. which is particularly important for the evaluation of human thermal stress as it corresponds to 2 *m* a.g.l. at full-scale which is close to human height (Fig. 3).

Air temperature and relative humidity were measured on the central axis of the street at 0.4 *m* a.g.l. and 1.5 *m* a.g.l. That is respectively under and inside the tree canopy. Both variables were also measured at the North mast at 2 *m* a.g.l. in order to carry out the calculation of the

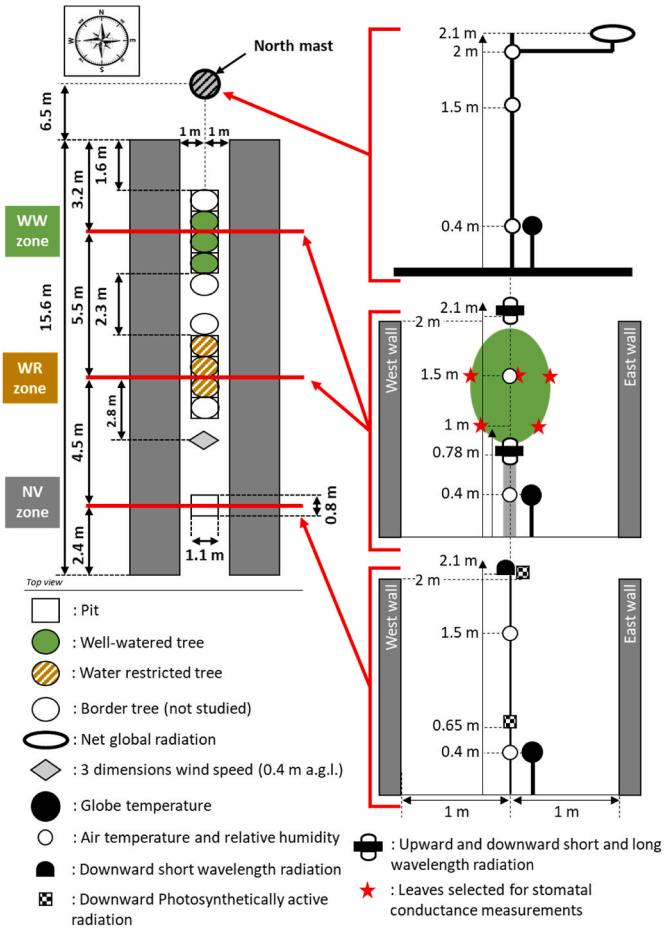

Fig. 3. Sketch of the studied street canyon showing the respective positions of the well-watered zone (WW), the water restricted zone (WR) and the non-vegetated zone (NV) with the location of the sensors in the different zones.

reference evapotranspiration presented hereinafter. The platinum and capacitive probes used for this measurement were placed in mechanically ventilated white painted cylindrical shelters. Both variables were used to compute the absolute humidity.

Globe temperature was measured at 0.4 *m* a.g.l. at the North mast as well as in each zone of the street on the central north-south axis using platinum probes mounted inside black painted copper spheres of 15 cm diameter.

The North mast was equipped with a net radiometer placed at 2.1 *m* a.g.l. inside the street, both vegetated zones were equipped with 4-components net radiometers placed at 0.78 *m* a.g.l. and 2.1 *m* a.g.l. that is just under and above the tree crowns respectively, to measure incident downward short wavelength radiation and its transmission through the tree crown. In the NV zone, the downward short wavelength radiation was measured at 2.1 *m* a.g.l. with a pyranometer and the Photosynthetically Active Radiation (PAR) was measured at 0.65 *m* and 2 *m* a.g.l. with PAR radiometers. PAR measurements were used to calculate the downward short wavelength radiation at 0.65 *m* a.g.l. In the NV zone as detailed in section 2.2.5.

The wind speed and direction on the studied site were measured outside the street at 2 *m* a.g.l. on the West mast with a 2D sonic anemometer, and inside the street with a 3D sonic anemometer at 0.4 *m* a.g.l. between the NV and WR zones at approximately 4.1 *m* from the south end of the street.

The on-site reference evapotranspiration was calculated with the meteorological variables measured outside the street at the North mast and West mast whereas the Universal Thermal Climate Index (UTCI) was calculated with the measurements carried out inside the street in order

to evaluate the human thermal stress at human height (0.4 *m* a.g.l. At reduced scale). The characteristics of the sensors used for the experiment are presented in appendix A and the methods used for the calculation are described in section 2.2.

2.1.4. Leaf area and crown projected area of the trees

The leaf area of the 3 central trees of each vegetated zone was estimated on July 7th and August 27th, 2022. For leaf-bearing axes, the length of all long axes (longer than 5 cm) was measured, the number of short axes was counted and the length and width of all leaves on a sample of 10 long and 10 short axes were measured. The area of each sampled leaf was calculated out of its length and width using an allometric relationship established on the basis of data acquired in previous experiments with the same experimental setup and the same trees (*Malus Coccinella*® 'Courtarou') giving one coefficient of leaf area per short axe and one per unit of foliated length for long axes. For each tree, the two coefficients were multiplied respectively by the number of short axes and the cumulative length of all long axes to compute the total leaf area.

The dimensions of the tree crowns were estimated for each zone by measuring the area of the horizontal rectangle encompassing the canopy of the 5 trees of each alignment. When divided by 5, this area was considered equal to the crown projected area on the ground per tree for each vegetated zone and was used to compute the Leaf Area Index (LAI) of each tree defined as the ratio of its total leaf area to its crown projected area. Linear interpolation and extrapolation were used to compute the crown projected area for each day of the studied period from July 8th and August 31st, 2022 on the basis of the values measured on July 7th and August 27th. From July 1st to July 6th, the crown projected area was considered equal to the one measured on July 7th. Indeed, the trees were pruned on June 23rd and their dimensions were supposed to remain constant during the two following weeks, i.e. from June 23rd to July 7th, 2022.

2.1.5. Stomatal conductance

Measurements of the stomatal conductance were carried out during 5 sunny, warm and rain-free days (July 5th, July 12th, July 19th, July 28th and August 9th, 2022) approximately with a 1-h time step on 5 mature leaves of the central tree of both vegetated zones with an AP4-UM-3 porometer (DeltaT Devices Ltd, Cambridge, UK). The 5 selected leaves were close to the edge of the tree crown in order to be exposed to the sun at least part of the day (Fig. 3). As the WR trees experienced defoliation, some of the selected leaves fell during summer and new leaves had to be selected. A daily average stomatal conductance value was calculated for each one of the 5 selected leaves from 10:00 to 12:00 UTC and was used to compute a daily average stomatal conductance for the central tree of each vegetated zone.

2.2. Methods

2.2.1. Irrigation control

Until July 4th, 2022, all trees were drip-irrigated every day between 20:00 and 22:00 UTC with an amount of water sufficient to guaranty that soil VWC was at field capacity (approx. 28 %) every night and that drainage water was collected on the following day. The irrigation dose was adjusted according to the forecasted meteorological conditions. Different indicators were monitored to ensure that the irrigation dose was sufficient to bring soil moisture at field capacity.

- The amount of drainage water collected every day was expected to be strictly positive;
- The water matric potential measured with the tensiometers was expected to be close to field capacity (−0.033 MPa) after evening irrigation;
- The soil VWC, measured with the capacitive probes, was expected to be close to field capacity (28 %) after evening irrigation.

On July 5th, 2022, two different irrigation treatments were applied to the two vegetated zones.

- The WW (well-watered) zone, located in the northern part of the street, was kept fully irrigated as described hereinabove all summer long in order to maintain the soil at field capacity.
- The WR (water-restricted) zone, located in the centre of the street, was subjected to a water restriction lasting until September 1st. The last full irrigation occurred on July 4th, in the evening. Thus, the trees were still experiencing comfortable water supplies on July 5th, and July 6th was considered as the first day of the restriction period (also called day 1). Then, a small irrigation dose was poured every day from July 7th included. The dose was chosen in order to maintain the soil VWC in the NR-AWS. In total the water restriction lasted for 8 weeks.

2.2.2. Estimation of tree transpiration with a water balance

A daily water balance was carried out on the basis of all water inputs and outputs of the tree containers in order to evaluate daily tree transpiration (1), and adapted for well-watered (WW) trees and water-restricted (WR) trees.

$$P + I - \Delta S - ETR - D \pm R = 0 \quad (1)$$

P is the total rainfall, I is the irrigation poured into the soil, ΔS is the variation of water storage in the soil, ETR is the effective evapotranspiration, D is the drainage water, R is the runoff, all expressed in litre. P and R can be considered null as trees are planted in containers covered with lids.

2.2.2.1. Estimation of tree transpiration for well-watered (WW) trees. The measurement of the daily drainage water (D) could not be carried out during non-working days (week-ends and public holidays). This is why the water balance was simplified (2) for well-watered trees on a daily time period delimited by the estimated start time and end time of tree diurnal transpiration as proposed by Mballo et al. [36] enabling to consider I and D null (Fig. 4). Night-time transpiration is considered null in this case as it was found to be low compared to the diurnal transpiration on different tree species [59,60].

$$ETR = -\Delta S_{daytime} = -\Delta\theta_{daytime}.V_{soil} \quad (2)$$

$\Delta\theta_{daytime}$ is the diurnal variation of the average soil VWC (points of %) calculated for each tree between the end time (approx. 19:30 UTC) and the start time (approx. 05:30 UTC) of diurnal transpiration using the two capacitive probes described in Fig. 2, V_{soil} (46.3 L) is the volume of topsoil-compost mixture poured in each container.

2.2.2.2. Estimation of tree transpiration for water-restricted (WR) trees. During the water restriction period, as the soil of the WR trees dries, the water distribution might become very heterogeneous preventing the two capacitive probes, which are very local sensors, to accurately represent the overall water distribution and dynamics in the soil. Indeed, the daily soil VWC variation of some WR trees became null until the end of the growing season, whereas they were still irrigated with small doses of water, and thus transpiring. To face this issue, the daily water balance of the WR trees was run on a 24-h time step (19:30 to 19:29 UTC next day) from July 6th until the end of the growing season. In this way, D was set to zero (it was checked that the amount of daily drainage water of the WR trees was null on this period) and I was included in the water balance which led simplify equation (1) as follows (3):

$$ETR = I - \Delta S_{24h} = I - \Delta\theta_{24h}.V_{soil} \quad (3)$$

Fig. 4 illustrates the daily water balance carried out in the present experiment and the hypotheses allowing the simplifications presented hereinabove.

The daily amount of water transpired by the trees was converted into

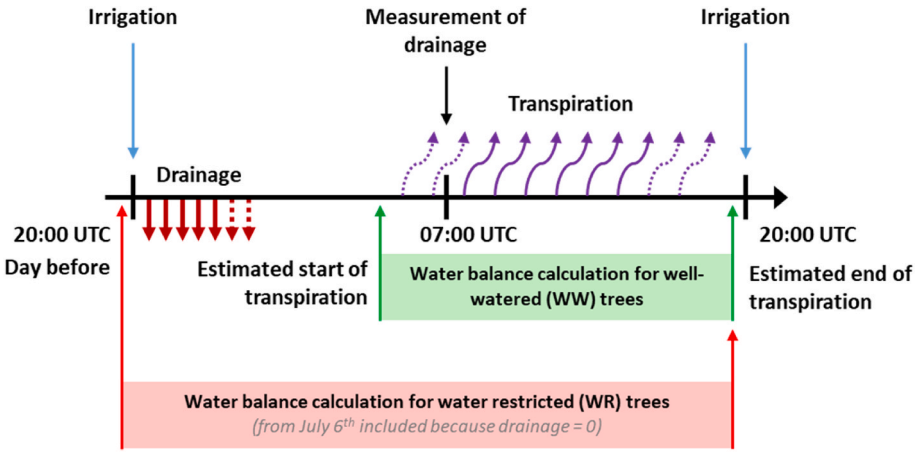

Fig. 4. Daily water inputs and outputs taken into account for the calculation of the water balance and daily tree transpiration (adapted from Mballo et al. [36]).

a daily quantity of energy consumed by the evaporation of water with the use of the latent heat of vaporization of vapour at 20 °C (2.46 MJ.kg^{-1}) and transformed to a quantity of energy per surface unit (MJ.m^{-2}.day^{-1}) using the average projected area of the tree crowns interpolated for each day as detailed in section 2.1.4.

2.2.3. Reference evapotranspiration

The daily reference evapotranspiration ET_{ref} was calculated on-site using the Penman-Monteith equation [58] in order to characterize the daily climatic conditions and to compare tree transpiration estimated with the water balance presented hereinabove to the climatic demand.

2.2.4. Insolation ratio

The daily insolation ratio was characterized by computing the ratio of the daily integral of the incident global radiation on top of the studied street canyon R_{top_street}, measured at 2.1 *m* a.g.l. using the pyranometer located in the NV zone of the street, to the daily integral of the theoretical solar radiation received by the earth above the atmosphere R_{top_atm} (reported by FAO et al. [58]) as proposed by Mballo et al. [36] in equation (4).

$$Insolation\ ratio = \frac{R_{top_{street}}}{R_{top_{atm}}} \tag{4}$$

The days were considered sunny when the insolation ratio exceeded 0.65 and cloudy when it was lower than 0.45 [36].

2.2.5. Downward short wavelength radiation intercepted by the tree crowns

The downward short wavelength radiation was monitored at various locations inside and outside the street canyon enabling to estimate the amount of radiation intercepted by the tree crowns. In the NV zone, the Photosynthetically Active Radiation (PAR) measured at 0.65 *m* a.g.l. was used to compute the downward short wavelength radiation at this height. To do so, the measurements of downward short wavelength radiation and PAR carried out on top of the NV zone (respectively at 2.1 *m* and 2 *m* a.g.l.) were used to compute the proportion of PAR in the global incident radiation at every time step (10 min) as this ratio may vary with the hour, date and location [61]. Then, this ratio was applied to the PAR measured at 0.65 *m* a.g.l. at each time step in the NV zone as presented in equation (5).

$$R_{10min-0.65m-NV} = PAR_{10min-0.65m-NV} \times \frac{R_{10min-2.1m-NV}}{PAR_{10min-2m-NV}} \tag{5}$$

$R_{10min\text{-}0.65m\ -\ NV}$ and $R_{10min\text{-}2.1m\ -\ NV}$ are the downward short wavelength radiation calculated at 0.65 *m* a.g.l. and measured at 2.1 *m* a.g.l. in the NV zone at each time step, $PAR_{10min\text{-}0.65m\ -\ NV}$ and $PAR_{10min\text{-}2m\ -\ NV}$ are the PAR measured respectively at 0.65 *m* and 2 *m* a.g.l. in the NV zone at each time step.

Then, in order to compute the amount of radiation intercepted by the tree crowns, the difference of the daily integral of the short wavelength radiation calculated at 0.65 *m* a.g.l. in the NV zone and measured at 0.78 *m* a.g.l. In both vegetated zones was computed and compared to the daily total amount of radiation calculated in the NV zone through the calculation of a ratio presented in equations (6) and (7).

$$r_{inter.crownWW} = \frac{R_{0.65m-NV} - R_{0.78m-WW}}{R_{0.65m-NV}} \tag{6}$$

$$r_{inter.crownWR} = \frac{R_{0.65m-NV} - R_{0.78m-WR}}{R_{0.65m-NV}} \tag{7}$$

$R_{0.78m\ -\ WW}$, $R_{0.78m\ -\ WR}$ and $R_{0.65m\ -\ NV}$ are the daily integral of the downward short wavelength radiation in MJ.m^{-2}.day^{-1} measured at 0.78 *m* a.g.l. in the WW zone, the WR zone and 0.65 *m* a.g.l. in the NV zone and $r_{inter.crownWW}$ and $r_{inter.crownWR}$ are the ratios of the daily integral of the short wavelength radiation intercepted by the crown of each vegetated zone (no unit).

2.2.6. Universal Thermal Climate Index (UTCI)

The Universal Thermal Climate Index (UTCI) was calculated at human height (0.4 *m* a.g.l. at reduced scale) following the methodology developed by Bröde et al. [62] using a 6th order polynomial regression function included in the version a0.002 of the calculation program released in October 2009 by Peter Bröde. This indicator was chosen because it takes into account all microclimate variables and an advanced human physiological model which parameters have been described by Fiala et al. [63,64] and Jendritzky et al. [65]. UTCI also has the advantage to be valid for a wide range of climatic conditions. UTCI was calculated at 0.4 *m* a.g.l. on the basis of the measurements of air temperature, air relative humidity and wind speed all carried out at the same location and on the calculation of the mean radiant temperature (T_{mrt}) with equation (8) [66].

$$T_{mrt} = \sqrt[4]{(T_g + 273.15)^4 + \frac{1.06 \times 10^8 \times V_a^{0.58}}{\varepsilon \times D^{0.42}}(T_g - T_a)} - 273.15 \tag{8}$$

T_{mrt}, T_g and T_a are respectively the mean radiant temperature, the globe temperature and the air temperature in °C calculated and measured at the chosen location (Fig. 3). E and D are respectively the globe emissivity (0.95) and diameter (0.15 *m*), and V_a is the wind speed measured in m.s^{-1} at 0.4 *m* a.g.l with the 3D sonic anemometer between the vegetated and non-vegetated zone for inside street T_{mrt} assessment.

2.3. Framework

In the present work, the two processes involved in the climatic

benefits of street trees were assessed during an 8-week water restriction alongside related variables (Fig. 5): tree transpiration alongside soil volumetric water content, stomatal conductance and air absolute humidity in section 3.1 and radiation interception alongside total leaf area and LAI in section 3.2. The respective contributions of both tree transpiration and radiation interception were assessed from an energetic point of view through an energy balance presented in section 3.3. Finally, the climatic benefits (air temperature and UTCI reduction) provided by both the WW and WR trees were compared in section 3.4.

3. Results

3.1. Impact of soil VWC on tree transpiration

During the studied period, in the WW zone, the irrigation event was followed by a quick increase of the VWC which was close to the field capacity (approx. 28 %) every night (Fig. 6). Then, the VWC quickly decreased during the night as part of the water was drained in depth in the container. Drainage water was collected every day which confirmed that the water supply was sufficient to cover the tree transpiration. During daytime, water was pumped by the trees for their transpiration leading to a noticeable decrease of the VWC. The R-AWS was totally consumed most of the time at the end of the day before irrigation.

In the WR zone, the same behaviour was observed before the beginning of the water restriction. Starting from July 6th, the soil VWC decreased and quickly approached the permanent wilting point (approx. 10 %). The small doses of water poured each day starting from July 7th enabled to maintain the VWC in the NR-AWS from July 6th and lower than 16 % at night after irrigation from July 14th with lower amplitudes of VWC variations compared to the WW zone. From August 15th, the irrigation dose poured to the WR trees was reduced as the reference evapotranspiration and insolation ratio were lower in order to prevent an increase of the soil VWC. Then, the soil VWC of the WR trees reached values even lower, close to the permanent wilting point, and the amplitude of the daily variations was also reduced.

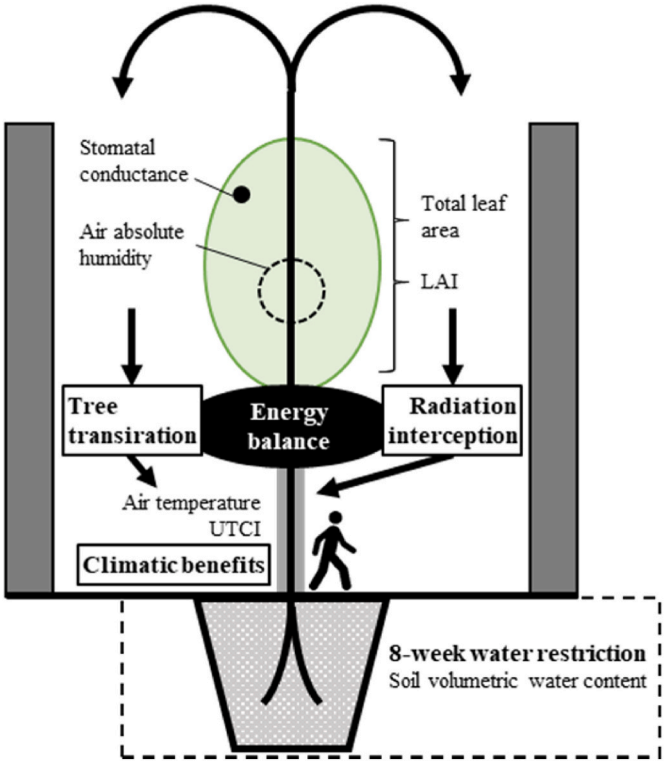

Fig. 5. Sketch representing the framework of the study.

Before the water restriction started, both vegetated zones were characterized by similar transpiration rates (Fig. 7a). The WR trees transpired on average 2.9 L.tree^{-1}.day^{-1} and the WW trees 2.4 L.tree^{-1}.day^{-1} which is slightly higher than the well-watered *Malus Coccinella*® 'Courtarou' of comparable LAI (2.5 m^2 m^{-2}) studied in 2020 by Mballo et al. [36] in the same experimental facility during a sunny day (2.0 L.tree^{-1}.day^{-1}) with a 0.5 mm lower reference evapotranspiration. At full scale, Caspari et al. [45] measured higher transpiration rates (from 3 to 4.8 L.tree^{-1}.day^{-1}) for two well-watered 5-year old Asian pear trees (*Pyrus serotine*) but with trees having a higher leaf area (6 m^2.tree^{-1}).

The beginning of the water restriction led to a quick and strong reduction of the transpiration of the WR trees. From July 6th to August 31st, the WR trees transpired on average 0.5 L.tree^{-1}.day^{-1} which is 81 % less than the WW trees (3 L.tree^{-1}.day^{-1} on average).

The daily average stomatal conductance of the central WW tree ranged from 5.7 to 12.1 mm.s^{-1} and appeared to be influenced by the daily meteorological conditions (Fig. 7b). On July 5th and 12th, the reference evapotranspiration and the cumulated incident radiation were high (respectively 3.7 and 4.3 mm.day^{-1} and 28.3 and 27.0 MJ.m^{-2}.day^{-1}) which led to a high stomatal conductance for the WW tree exceeding 10 mm s^{-1}. Conversely, the reference evapotranspiration and the incident radiation were low on July 28th and August 9th (respectively 2.8 and 2.9 mm.day^{-1} and 18.0 and 21.7 MJ.m^{-2}.day^{-1}) which led to a lower stomatal conductance of 5.7 and 6.5 mm.s^{-1} respectively. July 19th however was marked by a high stomatal conductance in spite of low reference evapotranspiration and incident radiation.

The stomatal conductance of the WR tree was already lower than the one of the WW tree on July 5th (5.7 mm.s^{-1} compared to 12.1 mm.s^{-1}) but the difference was statistically significant according to the Welch's *t*-test only from July 12th when the stomatal conductance of the WR tree collapsed to 1.1 mm.s^{-1} before remaining lower than 0.6 mm.s^{-1} during the next measurement days. Such values are consistent with those already reported in the literature. Konarska et al. [48] measured midday stomatal conductance ranging from approximately 1.5 to 5 mm.s^{-1} for 7 species of street trees but could not control their access to water. Bréda et al. [67] measured approximately 8 mm.s^{-1} for well-watered trees and 1 mm.s^{-1} or less for water-stressed trees when studying *Quercus petraea* and *Quercus robur*.

The air absolute humidity was calculated in the centre of the tree canopy of each zone at 1.5 *m* a.g.l. and averaged around noon (from 11:00 to 13:00 UTC) when the trees are fully exposed to sunlight (Fig. 7c). Before the start of the water restriction, the average absolute humidity was 7.9 $g_{water}.kg^{-1}_{dry\ air}$ in the NV zone, 8.2 $g_{water}.kg^{-1}_{dry\ air}$ in the WW zone and 8.1 $g_{water}.kg^{-1}_{dry\ air}$ in the WR zone meaning that the average absolute humidity was 0.5 % lower in the WR zone compared to the WW one (see the evolution of the absolute humidity difference between both vegetated zones in appendix C). Then, a noticeable difference of air absolute humidity between the two vegetated zones appeared during the water restriction and reached its maximal value on July13th (day 8 of the water restriction). On that day, the average absolute humidity was 7.4 $g_{water}.kg^{-1}_{dry\ air}$ in the NV zone, 8.1 $g_{water}.kg^{-1}_{dry\ air}$ in the WW zone and 7.2 $g_{water}.kg^{-1}_{dry\ air}$ in the WR zone which means that the absolute humidity was 11.4 % lower in the WR zone compared to the WW one. The difference between both zones was less important in August but an average difference of −4.7 % was calculated over the whole restriction period which means that the concentration of water vapour was less important in the surrounding air of the WR trees compared to that of the WW trees.

3.2. Impact of water restriction on leaf area and radiation interception

The values of leaf area, crown projected area and LAI measured in both vegetated zones at the beginning and at the end of the water restriction are presented in Table 1. The LAI measured in the WW and WR zones were close to those reported in other full-scale studies. Shahidan et al. [19] studied for instance *Mesua ferrea* L. and *Hura crepitans* L. with

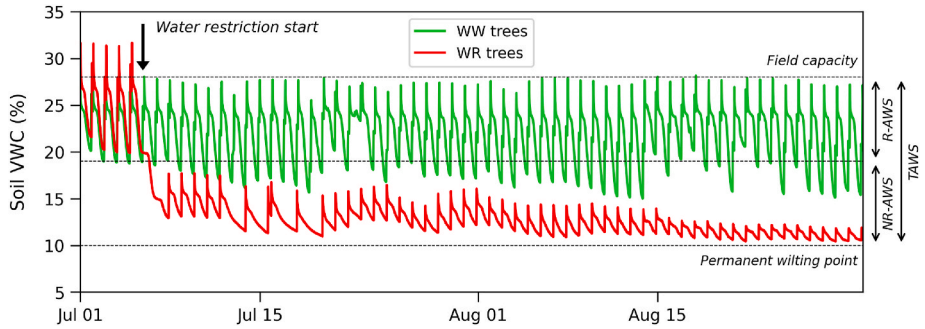

Fig. 6. Evolution of the average soil volumetric water content (VWC) measured for 3 well-watered (WW) trees and 3 water-restricted (WR) trees during July and August 2022. Each tree was equipped with 2 soil water content sensors. Maximum standard deviation is 6.5 % for both WW trees and WR trees (n = 6 capacitive probes for each zone). The ranges of soil VWC for the total available water storage (TAWS), the readily available water storage (R-AWS) and the non-readily available water storage (NR-AWS) are displayed.

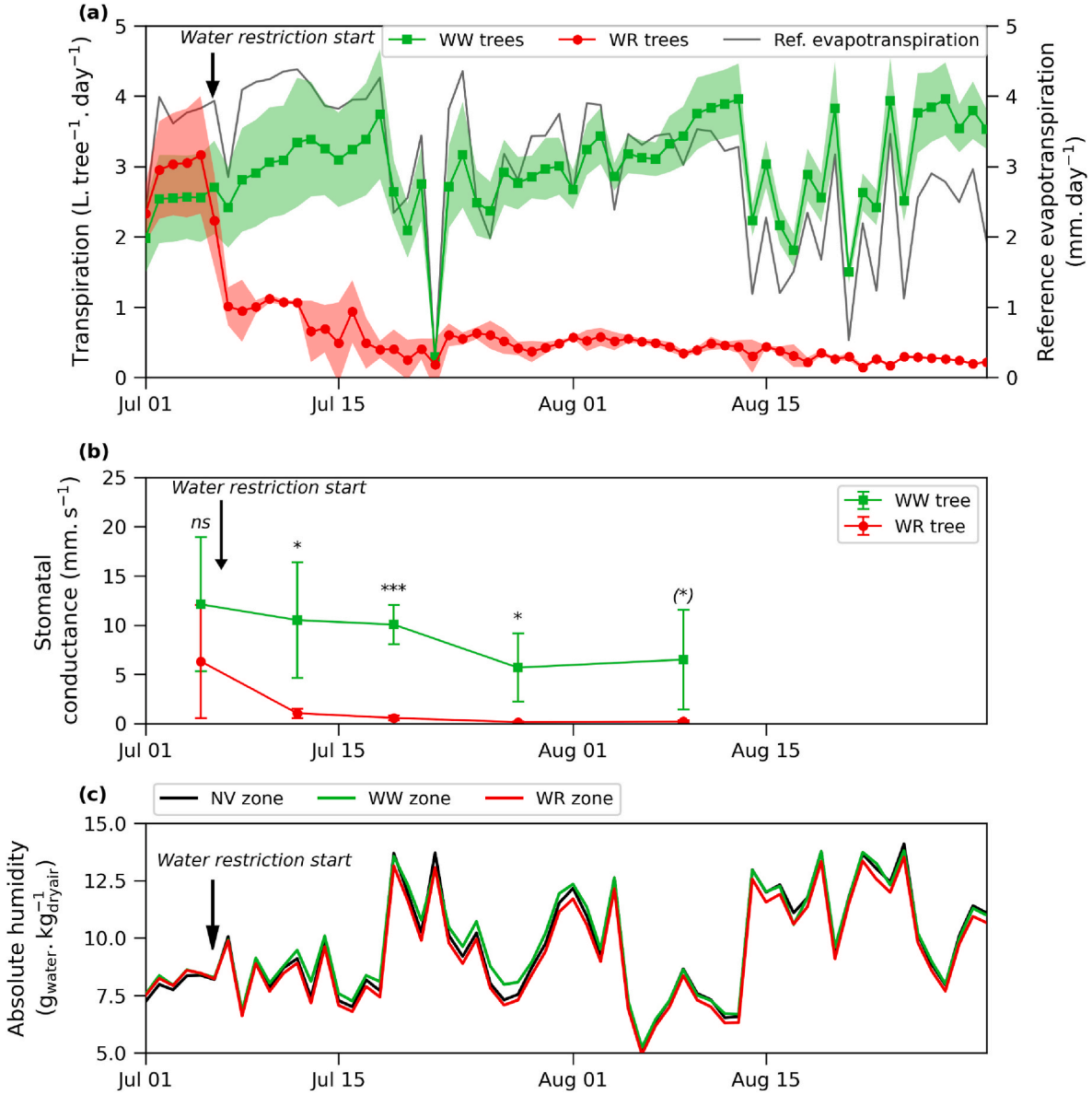

Fig. 7. Evolution during July and August 2022 of: (a) the reference evapotranspiration calculated at the North mast and the average daily tree transpiration and the associated standard deviation (n = 3) calculated for 3 well-watered (WW) trees and 3 water restricted (WR) trees. (b) The daily average stomatal conductance and the associated standard deviation measured on 5 leaves of the central tree of each zone from 10:00 to 12:00 UTC. Results of the daily Welch's *t*-test comparing the means of both vegetated zones are displayed (n = 5 leaves): ns: p > 0.1, (*): 0.1 ≥ p > 0.05, *: 0.05 ≥ p > 0.01, ***: 1.0e-3 ≥ p > 1.0e-4. (c) The absolute humidity calculated at 1.5 *m* a.g.l. Around noon (from 11:00 to 13:00 UTC) in the three zones of the street.

Table 1
Average total leaf area, crown projected area and Leaf Area Index (LAI) per tree (± standard deviation) measured during summer 2022 in the well-watered zone (WW) and the water-restricted zone (WR).

Date	WW zone			WR zone		
	Leaf area (m^2.tree^{-1})	Crown projected area (m^2)	LAI (m^2.m^{-2})	Leaf area (m^2.tree^{-1})	Crown projected area (m^2)	LAI (m^2.m^{-2})
July 7th, 2022	2.6 (±0.2)	1.1	2.4 (±0.2)	2.5 (±0.2)	1.1	2.4 (±0.2)
August 27th, 2022	4.4 (±0.3)	1.3	3.3 (±0.2)	1.8 (±0.0)	1.0	1.7 (±0.0)

LAI ranging from 1.5 to 6.1. Therefore, the latent heat flux in the present study is comparable to the one expected at full-scale with trees having comparable LAI and under equal water availability and climatic conditions. During the studied period, the leaf area, crown projected area and LAI increased for the WW trees while these three variables decreased for the WR trees (Table 1).

Then, Fig. 8 presents the daily evolution of the portion of downward short wavelength radiation intercepted by the WW and WR trees calculated on the basis of the downward short wavelength radiation measured in the NV zone at 0.65 *m* a.g.l. as defined in section 2.2.5. Until July 5th, before the start of the water restriction, the WW and WR trees intercepted a similar portion of the radiation received at 0.65 *m* a.g.l. in the NV zone, respectively 82 % and 83 % (Fig. 8). Such results were found to be consistent with full scale results such as those from Shahidan et al. [19] who found from 79 % to 93 % radiation interception with the range of LAI mentioned hereinabove. Then, the radiation interception ratio of the WR trees slowly decreased and reached on average 76 % during August 2022, remaining over 69 % until the end of the studied period. At the same time, the ratio of radiation intercepted by the WW trees slowly increased and reached a plateau at 86 % on average of the incoming radiation in the end of July 2022, remaining lower than 90 % until the end of the studied period. During August 2022, the average difference recorded between both zones was 9.5 points of % and the maximum difference was 17 points of % (August 25th).

3.3. Energy balance approach

Following the methodology reported by Mballo et al. [36], the sum of the daily amount of short wavelength radiation intercepted (section 2.2.5) and the daily amount of energy consumed by the evaporation of the transpired water (section 2.2.2) was considered as a daily amount of energy dissipated by the trees and graphed in Fig. 9. The contribution of tree transpiration is also displayed and that of the radiation interception can be inferred as the difference between the total amount of energy dissipated and the contribution of transpiration.

The average total amount of energy dissipated by both vegetated zones were very close from July 1st to 5th (20.3 MJ.m^{-2}.day^{-1} with 5.7 MJ.m^{-2}.day^{-1} (29 %) attributed to transpiration for the WW zone compared to 21.6 MJ.m^{-2}.day^{-1} dissipated in total by the WR zone with 6.7 MJ.m^{-2}.day^{-1} (32 %) attributed to transpiration). Mballo et al. [36] calculated a slightly lower contribution of tree transpiration during a sunny day of summer 2020 with well-watered apple trees (26 %) but with a lower transpiration rate as mentioned in section 3.1.

In the WW zone, the total amount of energy dissipated by the trees remained on average close to 17.3 MJ.m^{-2}.day^{-1} all along summer with a slight increase of the contribution of transpiration which reached 35 % on average during August 2022.

In the WR zone, the total amount of dissipated energy noticeably decreased from 21.6 MJ.m^{-2}.day^{-1} (average from July 1st to 5th) to 10.9 MJ.m^{-2}.day^{-1} (average during August 2022) and most of this reduction was attributed to the reduction of the WR trees transpiration (−6 MJ.m^{-2}.day^{-1}). In August 2022, the total amount of energy dissipated by the WR zone was 37 % lower than that of the WW trees and 8.1 % of this total amount came from the evaporation of transpired water.

3.4. Climatic benefits of the trees

The air temperature and UTCI measured in the three zones at 0.4 *m* a.g.l. were averaged daily between 10:00 and 14:00 UTC during July and August 2022 (Fig. 10) as the maximum climatic benefits provided by the well-watered trees were measured at solar noon by Mballo et al. [36] in this street canyon. The differences between the WR zone and the WW zone (WR zone - WW zone) were also calculated and graphed in Fig. 10c.

From July 1st to 5th (i.e. before the water restriction), the mean air temperature measured around noon was on average 2.7 °C lower in the WW zone and 1.8 °C lower in the WR zone compared to the NV zone. Thus, the WR zone was on average 0.9 °C warmer than the WW zone. Indeed, a non-constant pre-existing difference approaching 0.9–1 °C on average between the sensors was noticed and has to be considered when comparing both vegetated zones. Such results fit in the range of diurnal air temperature reductions found in the literature (from 0.7 °C [26] to more than 5 °C [27]) and are consistent with the maximum 2.7 °C reduction measured at midday by Mballo et al. [36] for well-watered trees. In August 2022, the WR zone was on average 1.2 °C hotter than the WW one (these differences include the pre-existing difference mentioned earlier) and 1.3 °C hotter when focusing on the driest and sunniest days of August (11 days with no rainfall and an insolation ratio greater than 0.65). During these eleven days, the air temperature was on average 3.1 °C lower in the WW zone and 1.8 °C lower in the WR zone compared to the NV zone.

From July 1st to 5th, the UTCI was on average 6.3 °C lower in the WW zone and 5.7 °C lower in the WR zone compared to the NV zone which is consistent with the findings of other studies at full scale [30] and with the 8 °C UTCI reduction measured at midday during a sunny day by

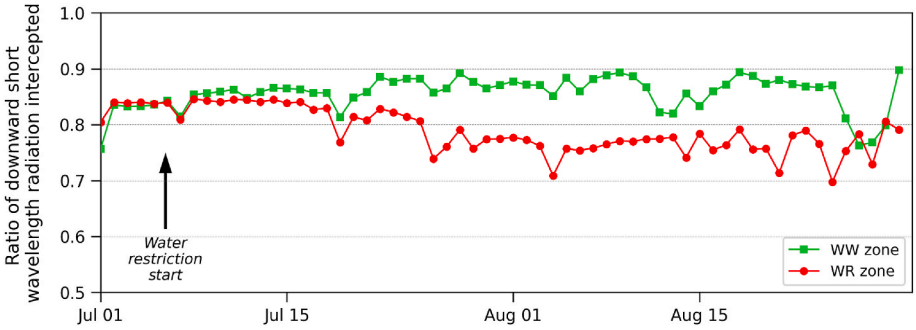

Fig. 8. Evolution of the ratio of the daily integral downward short wavelength radiation intercepted by the tree crowns calculated in the centre of both vegetated zones at 0.78 *m* a.g.l. On the basis of the daily integral incident radiation calculated in the non-vegetated (NV) zone at 0.65 *m* a.g.l.

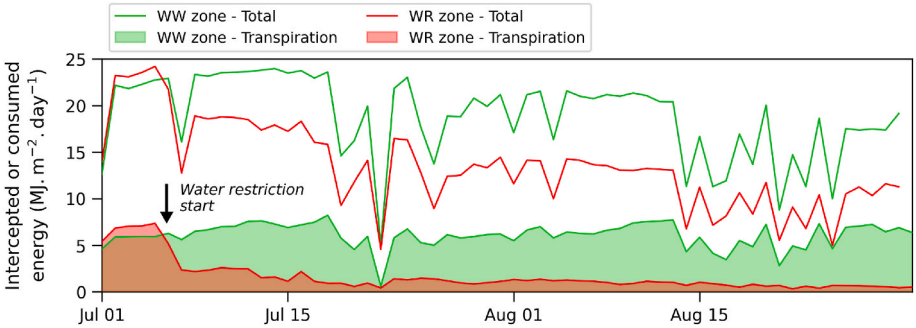

Fig. 9. Evolution of the daily amount of energy consumed by the tree transpiration and of the daily total amount of energy dissipated (consumed by the evaporation of transpired water + intercepted by the tree crowns) by each vegetated zone during summer 2022. The daily amount of radiative energy intercepted by the tree crowns can be inferred as the difference between the total amount and the amount related to transpiration.

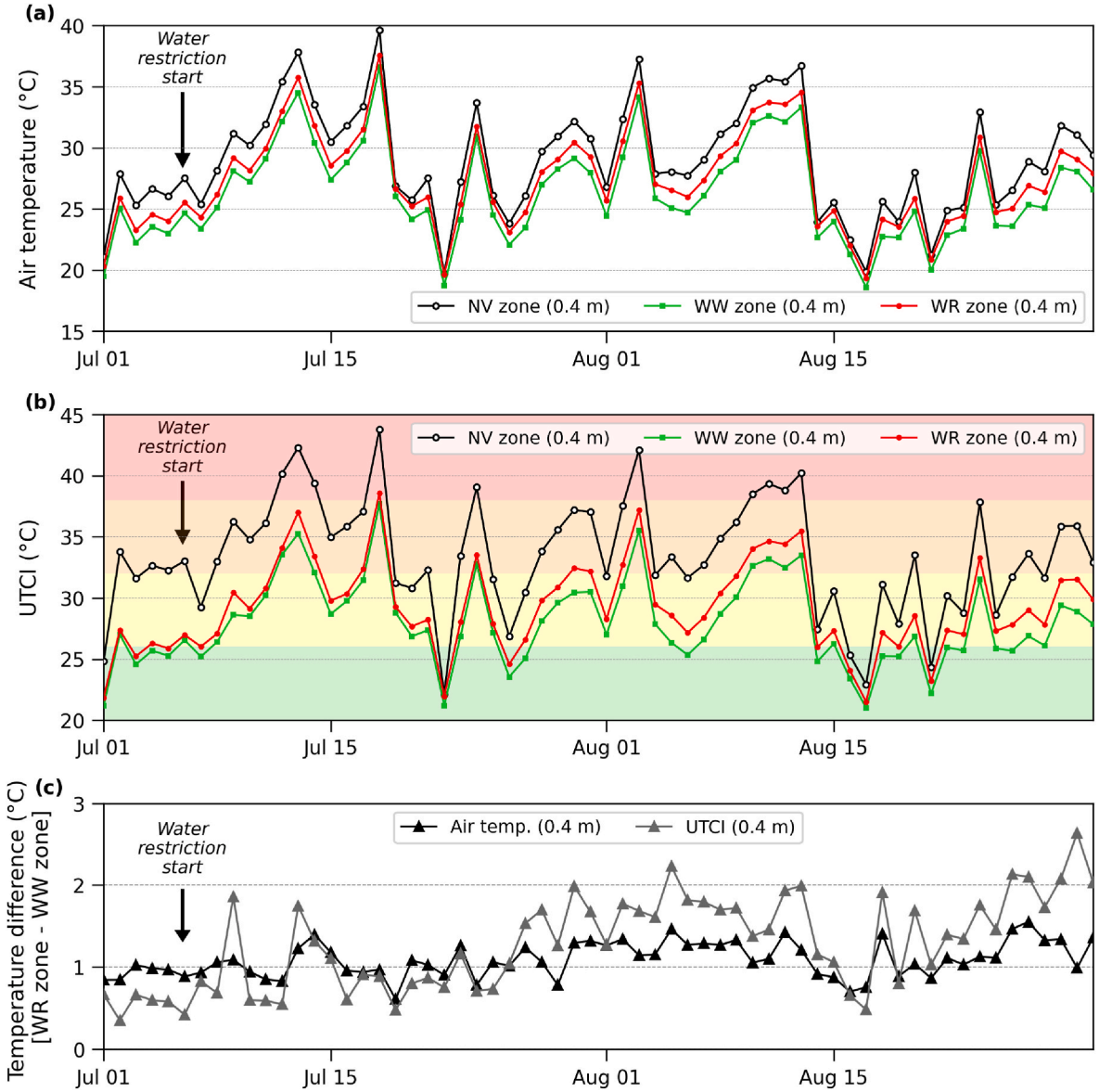

Fig. 10. Evolution of: (a) the air temperature measured at 0.4 *m* a.g.l. In each zone of the street and averaged from 10:00 UTC to 14:00 UTC; (b) UTCI calculated at 0.4 *m* a.g.l. In each zone of the street and averaged from 10:00 UTC to 14:00 UTC regarding the different thermal stress categories: no thermal stress (9–26 °C UTCI, green), moderate heat stress (26–32 °C UTCI, yellow), high heat stress (32–38 °C UTCI, orange), very high heat stress (38–46 °C UTCI, red) and extreme heat stress (>46 °C UTCI, not shown); (c) the difference of air temperature and UTCI between both vegetated zones (WR zone - WW zone) calculated daily between 10:00 and 14:00 UTC at 0.4 *m* a.g.l. During summer 2022. (For interpretation of the references to colour in this figure legend, the reader is referred to the Web version of this article.)

Mballo et al. [36] under well-watered trees in the present street canyon. The UTCI was on average 0.6 °C higher in the WR zone than in the WW one, which is probably caused by the pre-existing difference of air temperature mentioned hereinabove. During this period, the UTCI in the NV zone reached the high heat stress category almost every day unlike both vegetated zones which were maintained in the moderate heat stress category. During July and August 2022, the UTCI in the NV zone reached the very high heat stress category during 10 days whereas this category was reached only on July 18th in the WR zone and it was not reached in the WW zone. The UTCI difference between both vegetated zones increased along summer 2022. In August 2022, the UTCI was on average 1.6 °C higher in the WR zone compared to the WW one. This difference reaches 1.8 °C when focusing on the driest and sunniest days of August (11 days with no rainfall and an insolation ratio greater than 0.65). During these eleven days, the UTCI was on average 6.3 °C lower in the WW zone and 4.5 °C lower in the WR zone compared to the NV zone. At the end of August 2022, UTCI differences reaching up to 2.6 °C (July 30th) can be noticed between both vegetated zones.

4. Discussion

The present study relies on a reduced scale experimental facility built in the frame of a wider research program aiming at studying the climatic benefits of street trees. So far, only data acquired in 2020 and 2021 relying on well-watered trees [36,37,68] or during a preliminary study [50] with a very short water restriction (1 week) were partially released. Thus, the present contribution investigates, for the first time, the impact of a long water restriction (8 weeks) on street trees climatic benefits using new experimental data acquired over summer 2022. In this section, we discuss how the present study highlights the effect of a water restriction first on tree transpiration and radiation interception, then on the respective contributions of both processes from an energetic point of view and finally on the climatic benefits provided by street trees. Some limitations of the present experimental facility are also discussed and propositions to deepen the analyses are made.

The WW trees were not limited by water availability, allowing an increase over time of their leaf area, crown projected area and LAI as well as of their radiation interception ratio and transpiration (4 L.tree^{-1}.day^{-1} during the very last days of August compared to 2.4 L.tree^{-1}.day^{-1} in the beginning of July). However, even though on-site observations reported that the leaf area of the WW trees was still increasing in August 2022, their radiation interception did not exceed 90 %, meaning that they may have reached a maximal radiation interception capacity that cannot be exceeded even with a greater leaf area. Chen et al. [34] highlighted this threshold effect on various microclimatic variables through a numerical parametric study. Also, the lower insolation ratio observed around mid-August led to a slight decrease of the amount of radiation intercepted by the WW trees which induced an increase of the relative contribution of transpiration to the climatic benefits.

Conversely, the WR trees transpiration was strongly and quickly reduced: it reached already half that of the WW trees on the second day of restriction and was on average 81 % lower than that of the WW trees during the entire water restriction period (Fig. 7) which recalls the findings of Caspari et al. [45] and Tan et al. [46] mentioned in the introduction section. The tree transpiration seemed to be highly driven by the daily reference evapotranspiration when considering WW trees whereas the transpiration of the WR trees appeared to be limited by the daily amount of water poured through the controlled irrigation. Such results were very consistent with the quick partial closure of the WR trees stomata, also observed by Konarska et al. [48] and Gebauer et al. [47] during dry periods, as well as the decreasing amount of water vapour measured into the atmosphere of the WR tree crowns (Fig. 7). The crown projected area of the WR trees remained almost constant during the studied period suggesting that the crown stopped expanding horizontally early in the summer, meanwhile the leaf area and the LAI decreased (29 % reduction for the LAI), likely due to partial defoliation observed on-site (Table 1), which was consistent with the results of Dervishi et al. [49] who found lower foliage density for water-restricted trees compared to well-watered ones. Such LAI reduction led to a decrease of their radiation interception ratio (Fig. 8) on average from 83 % to 76 % (8 % reduction) which recalls the relationship between LAI and radiation interception highlighted by Shahidan et al. [19]. Still, their remaining leaf area and stems appeared to be sufficient to intercept at least 69 % and on average 76 % of the radiation measured in the NV zone during August 2022. As a consequence, the total amount of energy dissipated by the WR trees noticeably decreased and most of this reduction was attributed to the reduction of the WR trees transpiration although transpiration was only responsible for one third of the total amount of energy dissipated for trees experiencing well-watered conditions (Fig. 9).

Nevertheless, the WR zone kept providing noticeable climatic benefits until the end of the studied period in spite of the lack of water, mainly because it maintained its shading potential. Taking into account that air temperature and UTCI were slightly higher in the WR zone compared to the WW zone at the beginning of the studied period, the net difference of air temperature measured between both vegetated zones at 0.4 *m* a.g.l. increased by about 0.3 °C (Fig. 10) which is almost negligible compared to the sensors accuracy (±0.2 °C, see Table A1). The net difference of UTCI increased by approximately 1 °C, which is noticeable but still low regarding the amplitude of the thermal stress categories defined for the UTCI interpretation (e.g. the moderate heat stress ranges from 26 to 32 °C UTCI).

Tree transpiration was much more impacted by the water restriction than radiation interception. Yet, the lower contribution of tree transpiration to energy dissipation may explain the low climatic impact of the water restriction observed between both vegetated zones. Also, the transpiration-related energy dissipation is located at the leaves surface right where the transpiration occurs. Yet, the assessment of the climatic benefits of the trees was carried out under the tree crowns at 0.4 *m* a.g.l. (equivalent human height). At this location, the cooling effect of the evaporation of the transpired water is likely to be lower than inside the tree crowns where the latent heat flux takes place, which may explain the low impact of the water restriction on air temperature. This could suggest that the air temperature reduction provided by the trees under their crown compared to the NV zone may be more related to the interception of the incident radiation, which prevents the street surfaces from overheating, than to the evaporation of the transpired water.

The thermal comfort index (UTCI) relies on the measurement of globe temperature (through the mean radiant temperature) which is very sensitive to short wavelength radiation. Thereby, the LAI reduction observed in the WR zone, which caused the slight decrease of radiation interception, is very likely to have induced an increase of globe temperature (data not shown) in this zone causing the UTCI difference increase between both vegetated zones. Indeed, a lower foliage density was already related to a lower cooling potential of trees especially regarding human thermal stress mitigation [69]. Yet, it is likely that the decrease of radiation interception in the WR zone was too low to induce a significant increase of the ground surface temperature and of the sensible convective heat transfers which would have led to a noticeable increase of air temperature in the WR zone. This suggests that preserving the shadows cast by the trees is essential to prevent human thermal stress from increasing during a water restriction.

Yet, the present results have to be considered in the frame of the limitations associated to the present experimental facility. This reduced scale facility enabled to perform continual monitoring and to guaranty the homogeneity of some parameters such as building heights and surface materials. However, the three studied zones of the present street were located close from each other which is why some interactions may exist between them although some precautions were taken to limit these eventual interactions as explained in section 2.1 (orientation of the street perpendicular to the prevailing winds, meteorological sensors mounted at the centre of each zone). For instance, the WR zone being

located right next to the NV zone, the overheating of the NV zone may be transferred from the NV zone to the WR zone. However, the effect of such interactions were very likely to be low as shown by a previous study performed in the same experimental facility in the frame of the work of Mballo [70] which showed that the microclimate differences between the vegetated and non-vegetated zones of the street were not affected by wind direction by comparing 12 sunny days with contrasted wind speeds and directions.

The comparison of the results with full-scale studies is also not trivial. However, Mballo et al. [36] have already brought various answers to this aspect and the present results were found to be consistent with various full-scale studies, as shown in the results section.

Also, the present measurements carried out under the tree crowns may have been too local to show the entire effect of the increase of the radiation transmitted by the WR trees on the temperature of the surrounding ground and building facades which may have modified both the buildings energy budget as well as human thermal stress in other parts of the street (Fig. 9). Thus, it is important to assess the role of the crown of WR trees in the complete radiation balance of the street. To do so, the use of infrared imaging to assess the area of shaded street surfaces or the evaluation of the street surfaces temperature as well as the upward and downward short and long wavelength radiation with a thinner time step during both daytime and night-time could be interesting. Also, the effect of water restriction on UTCI being mainly mediated by radiation interception, the effect of water restriction on crown architecture should be further investigated to understand how it impacts axis and leaf growth as well as defoliation in relation with climatic benefits, especially as different tree species could have contrasted architectures and responses [17,71].

5. Conclusion

The present study enabled to evaluate the influence of a long water restriction (8 weeks during summer season with soil VWC in the lower zone of non-readily available water storage) on the climatic benefits of street trees in a 1/5 scale street canyon. The impact on tree transpiration was quick and strong. A noticeable reduction of the LAI of the WR trees led to a slight decrease of their radiation interception which however remained high. Although the daily total amount of energy dissipated by the WR trees was noticeably reduced, the WR trees maintained efficient cooling benefits all along the water restriction period. No noticeable air temperature difference was measured under the tree crowns of both zones at 0.4 m a.g.l. (equivalent to human height at full scale) but the difference of UTCI calculated under the tree crowns at 0.4 m a.g.l. between the WR trees and the WW trees increased from 0.6 °C before the water-restriction to 1.6 °C in the end of the studied period. The differences of climatic benefits provided by both WW and WR trees remained low which is consistent with the low impact of the water restriction on the radiation interception of the WR trees, since radiation interception is responsible for the major part of the daily total amount of energy dissipated by the trees. The present work should be completed with the monitoring of complementary variables (surface temperatures, long wavelength radiation fluxes, etc.) and with deeper analyses on a daily cycle to understand the role of the crown of WR trees in the complete radiation balance of the street. Such results could enable to improve the accuracy of the numerical models which are increasingly used to assess the effect of trees on the urban climate but to date do not take into account water stress. The present work should also be extended to other tree species in order to help stakeholders select the most adapted tree species regarding both the resistance to drought and the overheating mitigation in cities especially during heatwaves.

CRediT authorship contribution statement

J. Thierry: Writing – review & editing, Writing – original draft, Visualization, Validation, Software, Investigation, Formal analysis, Data curation. **S. Herpin:** Writing – review & editing, Validation, Supervision, Software, Project administration, Methodology, Funding acquisition, Formal analysis, Data curation, Conceptualization. **R. Levi:** Investigation, Formal analysis, Data curation. **D. Canonne:** Writing – review & editing, Investigation, Data curation. **S. Demotes-Mainard:** Writing – review & editing, Validation, Methodology, Conceptualization. **P. Cannavo:** Writing – review & editing, Methodology. **D. Lemesle:** Software, Resources. **L. Brialix:** Writing – review & editing, Software, Resources. **F. Rodriguez:** Writing – review & editing, Validation, Supervision, Methodology, Conceptualization. **P.E. Bournet:** Writing – review & editing, Validation, Supervision, Project administration, Methodology, Funding acquisition, Conceptualization.

Declaration of competing interest

The authors declare that they have no known competing financial interests or personal relationships that could have appeared to influence the work reported in this paper.

Data availability

Data will be made available after a 2-year period of time enabling to complete the analysis of the entire dataset.

Acknowledgements

This work took place within the framework of a thesis funded by the City of Paris, the French Ministry of Education, Research and Innovation through the ANRT, France (National Association for Research and Technology). This project also benefited from the financial support of the regional program “Objectif Végétal, Research, Education and Innovation in Pays de la Loire”, managed by the French Region Pays de la Loire, Angers Loire Métropole and the European Regional Development Fund. Our thanks also go to Yvette Barraud-Roussel (EPHor, Institut Agro Rennes-Angers) who drew the experimental water retention curve used for the soil characterization and to Bénédicte Dubuc, Lydie Ledroit and Camille Lebras (Univ Angers, Institut Agro, INRAE, UMR IRHS) for measurements concerning the trees. We finally warmly thank the staff of the Phenotic platform and IRHS for their help in this project as well as the nursery André Briant Jeunes Plants who supplied the trees used for this experiment.

Appendix A. Characteristics of the sensors

Table A1
Characteristics of the sensors used for the experiment. Data-loggers were used to scan all sensors every 10 s and record average values every 10 min (n.c. = not communicated).

Measured variable	Sensor type	Measurement range	Accuracy	Reference, manufacturer
Volumetric water content (VWC)	Capacitive probe	0–100 %	±2 % (±0.02 cm^3/cm^3)	EC-5, Decagon
Water matric potential	Tensiometer	0 to −0.1 MPa	±0.2 %	STCP 850, SDEC
Air temperature	Platinum	−40 to +60 °C	±0.2 °C	HMT330 and HMP110, Vaisala
Air relative humidity	Capacitive	0–100 %	±1.5 % for HR ≤ 90 %	HMT330 and HMP110, Vaisala
Globe temperature	Platinum	−5 to +95 °C	±0.15 + 0.002 × T (°C)	PT100, RS Pro
Net radiation	Net radiometer	n.c.	±10 % on daily sum	NR Lite, Kipp&Zonen
Short and long wavelength radiation	4 components Net radiometer	n.c.	±10 % on daily sum	CNR1, CNR4, Kipp&Zonen
Short wavelength radiation	Pyranometer	n.c.	±10 % on daily sum	CMP3, Kipp&Zonen
Photosynthetically active radiation	Radiometer	400–700 nm	±1 %	LI-190SA, Li-Cor
Wind speed and direction	2D sonic anemometer	0–60 $m.s^{-1}$ 0–359°	±2 % (at 12 $m.s^{-1}$) ±3° (at 12 $m.s^{-1}$)	Mc Gill Windsonic
Wind speed and direction	3D sonic anemometer	0–30 $m.s^{-1}$ 0–359°	±0.08 $m.s^{-1}$ ±0.7° (at 1 $m.s^{-1}$)	CSAT-3D, Campbell Scientific

Appendix B. Meteorological conditions of the studied period

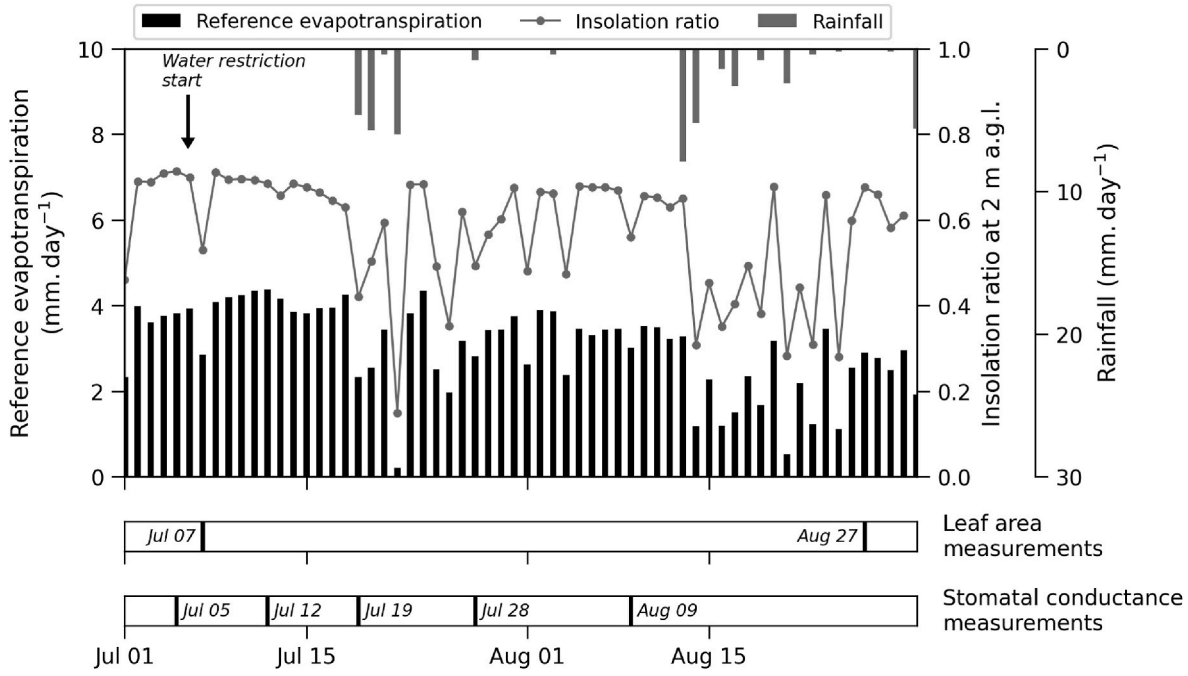

Fig. B1. Evolution of the reference evapotranspiration calculated at the North mast, the insolation ratio calculated above the street and the rainfall measured at the Météo-France meteorological station during July and August 2022. The multiple days of interest are highlighted below the figure.

Appendix C. Absolute humidity difference between both vegetated zones

The air absolute humidity was calculated in the centre of the tree canopy of each zone at 1.5 *m* a.g.l. and averaged around noon (from 11:00 to 13:00 UTC) when the trees are fully exposed to sunlight. The difference between the WW and WR zones was computed and expressed as a percentage of the absolute humidity calculated in the WW zone (Figure C1). A negative difference means that the absolute humidity is lower in the WR zone than in the WW zone. The average difference of absolute humidity between both zones was −0.5 % before the water restriction start. Then, it noticeably decreased to −11.4 % on July 13th (day 8 of the water restriction). The difference between both zones was less important in August but an average difference of −4.7 % was calculated over the whole restriction period. Which means that the concentration of water vapour was less important in the surrounding air of the WR trees compared to that of the WW trees.

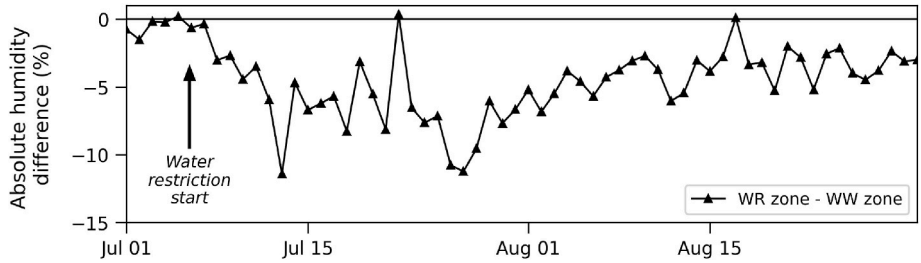

Fig. C1. Evolution during July and August 2022 of the absolute humidity difference between WR and WW zones calculated at 1.5 *m* a.g.l. Around noon (from 11:00 to 13:00 UTC) and expressed as a percentage of the absolute humidity measured in the WW zone.

References

[1] IPCC, Synthesis Report of the IPCC Sixth Assessment Report (AR6) 36, 2023.
[2] Météo-France, Vagues de chaleur et changement climatique, 2022 [WWW Document]. Météo-Fr. URL, https://meteofrance.com/changement-climatique/observer/changement-climatique-et-vagues-de-chaleur. (Accessed 4 March 2023).
[3] A.J. Arnfield, Two decades of urban climate research: a review of turbulence, exchanges of energy and water, and the urban heat island, Int. J. Climatol. 23 (2003) 1–26, https://doi.org/10.1002/joc.859.
[4] Y. Chen, B. Shan, X. Yu, Study on the spatial heterogeneity of urban heat islands and influencing factors, Build. Environ. 208 (2022), https://doi.org/10.1016/j.buildenv.2021.108604.
[5] T.R. Oke, Boundary Layer Climates, first ed., Routledge, London, 1978.
[6] J. Bouyer, Modélisation et simulation des microclimats urbains - Étude de l'impact de l'aménagement urbain sur les consommations énergétiques des bâtiments, Université de Nantes (2009).
[7] C. Sun, W. Lian, L. Liu, Q. Dong, Y. Han, The impact of street geometry on outdoor thermal comfort within three different urban forms in severe cold region of China, Build. Environ. 222 (2022), https://doi.org/10.1016/j.buildenv.2022.109342.
[8] M. Kuchcik, Mortality and thermal environment (UTCI) in Poland—long-term, multi-city study, Int. J. Biometeorol. 65 (2021) 1529–1541, https://doi.org/10.1007/s00484-020-01995-w.
[9] K. Laaidi, Rôle des îlots de chaleur urbains dans la surmortalité observée pendant les vagues de chaleur, Institut de veille sanitaire, 2012.
[10] H. Alsaad, M. Hartmann, R. Hilbel, C. Voelker, The potential of facade greening in mitigating the effects of heatwaves in Central European cities, Build. Environ. 216 (2022), https://doi.org/10.1016/j.buildenv.2022.109021.
[11] N. Zuckerman, I.M. Lensky, Thermal performance of vertical greenery systems (VGS) in a street canyon: a real-scale long-term experiment, Build. Environ. 244 (2023), https://doi.org/10.1016/j.buildenv.2023.110750.
[12] A. Frei, Thermal properties of green, white and other building roof materials and solar insolation: a case study in New York City, Build. Environ. 244 (2023), https://doi.org/10.1016/j.buildenv.2023.110842.
[13] X. Wang, G. Liu, N. Zhang, H. Liu, X. Tang, M. Lyu, H. Meng, Effects of cooling roofs on mitigating the urban heat island and human thermal stress in the Pearl River Delta, China, Build. Environ. 245 (2023), https://doi.org/10.1016/j.buildenv.2023.110880.
[14] J. Bernard, A. Gros, A. Rodler, B. Morille, M. Musy, P. Kéravec, S. Guernouti, COOLPARKS: Observation du rafraîchissement d'un parc nantais au-delà de son enceinte, in: Presented at the 35ème colloque annuel de l'Association Internationale de Climatologie, 2022. Toulouse, France.
[15] H. Liu, B. Huang, X. Cheng, M. Yin, C. Shang, Y. Luo, B.-J. He, Sensing-based park cooling performance observation and assessment: a review, Build. Environ. 245 (2023), https://doi.org/10.1016/j.buildenv.2023.110915.
[16] U.K. Priya, R. Senthil, A review of the impact of the green landscape interventions on the urban microclimate of tropical areas, Build. Environ. 205 (2021), https://doi.org/10.1016/j.buildenv.2021.108190.
[17] M.A. Rahman, L.M.F. Stratopoulos, A. Moser-Reischl, T. Zölch, K.-H. Häberle, T. Rötzer, H. Pretzsch, S. Pauleit, Traits of trees for cooling urban heat islands: a meta-analysis, Build. Environ. 170 (2020) 106606, https://doi.org/10.1016/j.buildenv.2019.106606.
[18] J. Konarska, F. Lindberg, A. Larsson, S. Thorsson, B. Holmer, Transmissivity of solar radiation through crowns of single urban trees—application for outdoor thermal comfort modelling, Theor. Appl. Climatol. 117 (2014) 363–376, https://doi.org/10.1007/s00704-013-1000-3.
[19] MohdF. Shahidan, M.K.M. Shariff, P. Jones, E. Salleh, A.M. Abdullah, A comparison of Mesua ferrea L. and Hura crepitans L. for shade creation and radiation modification in improving thermal comfort, Landsc. Urban Plann. 97 (2010) 168–181.
[20] S. Gillner, J. Vogt, A. Tharang, S. Dettmann, A. Roloff, Role of street trees in mitigating effects of heat and drought at highly sealed urban sites, Landsc. Urban Plann. 143 (2015) 33–42, https://doi.org/10.1016/j.landurbplan.2015.06.005.
[21] M. Sharmin, M.G. Tjoelker, S. Pfautsch, M. Esperon-Rodriguez, P.D. Rymer, S. A. Power, Tree crown traits and planting context contribute to reducing urban heat, Urban For. Urban Green. 83 (2023) 127913, https://doi.org/10.1016/j.ufug.2023.127913.
[22] D. Armson, P. Stringer, A.R. Ennos, The effect of tree shade and grass on surface and globe temperatures in an urban area, Urban For. Urban Green. 11 (2012) 245–255, https://doi.org/10.1016/j.ufug.2012.05.002.
[23] D. Armson, M.A. Rahman, A.R. Ennos, A comparison of the shading effectiveness of five different street tree species in manchester, UK, Arboric. Urban For. 39 (2013).
[24] L. Shashua-Bar, M.A. Rahman, A. Moser-Reischl, A. Peeters, E. Franceschi, H. Pretzsch, T. Rötzer, S. Pauleit, G. Winters, E. Groner, S. Cohen, Do urban tree hydraulics limit their transpirational cooling? A comparison between temperate and hot arid climates, Urban Clim. 49 (2023) 101554, https://doi.org/10.1016/j.uclim.2023.101554.
[25] S. Zheng, J.-M. Guldmann, Z. Wang, Z. Qiu, C. He, K. Wang, Experimental and theoretical study of urban tree instantaneous and hourly transpiration rates and their cooling effect in hot and humid area, Sustain. Cities Soc. 68 (2021) 102808, https://doi.org/10.1016/j.scs.2021.102808.
[26] C.A. Souch, C. Souch, The effect of trees on summertime below canopy urban climates: a case study, Bloomington, Indiana. J. Arboric. 19 (1993) 303–312.
[27] L.S. Vailshery, M. Jaganmohan, H. Nagendra, Effect of street trees on microclimate and air pollution in a tropical city, Urban For. Urban Green. 12 (2013) 408–415.
[28] P. Bröde, G. Jendritzky, D. Fiala, G. Havenith, The universal thermal climate index UTCI in operational use. Presented at the Adapting to Change: New Thinking on Comfort, 2010.
[29] M. Migliari, R. Babut, C. De Gaulmyn, L. Chesne, O. Baverel, The Metamatrix of Thermal Comfort: a compendious graphical methodology for appropriate selection of outdoor thermal comfort indices and thermo-physiological models for human-biometeorology research and urban planning, Sustain. Cities Soc. 81 (2022), https://doi.org/10.1016/j.scs.2022.103852.
[30] A.M. Coutts, E.C. White, N.J. Tapper, J. Beringer, S.J. Livesley, Temperature and human thermal comfort effects of street trees across three contrasting street canyon environments, Theor. Appl. Climatol. 124 (2016) 55–68, https://doi.org/10.1007/s00704-015-1409-y.
[31] T. Zhang, B. Hong, X. Su, Y. Li, L. Song, Effects of tree seasonal characteristics on thermal-visual perception and thermal comfort, Build. Environ. 212 (2022), https://doi.org/10.1016/j.buildenv.2022.108793.
[32] F. Ali-Toudert, H. Mayer, Thermal comfort in an east–west oriented street canyon in Freiburg (Germany) under hot summer conditions, Theor. Appl. Climatol. 87 (2007) 223–237, https://doi.org/10.1007/s00704-005-0194-4.
[33] J. Hang, D. Wang, L. Zeng, L. Ren, Y. Shi, X. Zhang, Scaled outdoor experimental investigation of thermal environment and surface energy balance in deep and shallow street canyons under various sky conditions, Build. Environ. 225 (2022), https://doi.org/10.1016/j.buildenv.2022.109618.
[34] T. Chen, N. Meili, F. Simone, J. Hang, P.Y. Tan, C. Yuan, Effects of tree plantings with varying street aspect ratios on the thermal environment using a mechanistic urban canopy model, Build. Environ. 111006 (2023), https://doi.org/10.1016/j.buildenv.2023.111006.
[35] J. Hang, G. Chen, Experimental study of urban microclimate on scaled street canyons with various aspect ratios, Urban Clim. 46 (2022), https://doi.org/10.1016/j.uclim.2022.101299.
[36] S. Mballo, S. Herpin, M. Manteau, S. Demotes-Mainard, P.E. Bournet, Impact of well-watered trees on the microclimate inside a canyon street scale model in outdoor environment, Urban Clim. 37 (2021) 100844, https://doi.org/10.1016/j.uclim.2021.100844.
[37] S. Herpin, S. Mballo, J. Thierry, D. Lemesle, L. Brialix, F. Rodriguez, S. Demotes-Mainard, P.-E. Bournet, Benefits of well-watered trees on street microclimate: what is the influence of meteorological conditions?. Presented at the 35th Annual Congress of the International Association of Climatology, 2022.
[38] A. Schütt, J.N. Becker, A. Gröngröft, S. Schaaf-Titel, A. Eschenbach, Soil water stress at young urban street-tree sites in response to meteorology and site parameters, Urban For. Urban Green. 75 (2022), https://doi.org/10.1016/j.ufug.2022.127692.
[39] H. Cochard, A. Granier, Fonctionnement hydraulique des arbres forestiers, Rev. For. Fr 51 (1999) 121–134.
[40] J. Lecoeur, Influence d'un déficit hydrique sur le fonctionnement d'un couvert végétal cultivé, 2007.
[41] O. Brendel, H. Cochard, Comment les espèces végétales s'adaptent au stress hydrique, in: L'Eau pour les Forêts et les Hommes en Région Méditerranéenne : un équilibre à trouver, What Science Can Tell Us, 2011.

[42] R. Zweifel, K. Steppe, F.J. Sterck, Stomatal regulation by microclimate and tree water relations: interpreting ecophysiological field data with a hydraulic plant model, J. Exp. Bot. 58 (2007) 2113–2131.
[43] N. Meili, J.A. Acero, N. Peleg, G. Manoli, P. Burlando, S. Fatichi, Vegetation cover and plant-trait effects on outdoor thermal comfort in a tropical city, Build. Environ. 195 (2021), https://doi.org/10.1016/j.buildenv.2021.107733.
[44] S. Chen, Z. Chen, Z. Feng, Z. Kong, H. Xu, Z. Zhang, Species difference of transpiration in three urban coniferous forests in a semiarid region of China, J. Hydrol. 617 (2023) 129098, https://doi.org/10.1016/j.jhydrol.2023.129098.
[45] H.W. Caspari, S.R. Green, W.R.N. Edwards, Transpiration of well-watered and water-stressed Asian pear trees as determined by lysimetry, heat-pulse, and estimated by a Penman-Monteith model, Agric. For. Meteorol. 67 (1993) 13–27, https://doi.org/10.1016/0168-1923(93)90047-L.
[46] P.Y. Tan, N.H. Wong, C.L. Tan, S.K. Jusuf, K. Schmiele, Z.Q. Chiam, Transpiration and cooling potential of tropical urban trees from different native habitats, Sci. Total Environ. 705 (2020) 135764, https://doi.org/10.1016/j.scitotenv.2019.135764.
[47] R. Gebauer, D. Volařík, K. Houšková, M. Matoušková, Z. Paschová, J. Štykar, R. Vitásek, J. Urban, R. Plichta, Sensitivity of physiological traits to different short-term drought events and subsequent recovery at the sapling stage in European white elm (Ulmus laevis Pall.), Environ. Exp. Bot. 214 (2023) 105469, https://doi.org/10.1016/j.envexpbot.2023.105469.
[48] J. Konarska, J. Uddling, B. Holmer, M. Lutz, F. Lindberg, H. Pleijel, S. Thorsson, Transpiration of urban trees and its cooling effect in a high latitude city, Int. J. Biometeorol. 60 (2016) 159–172, https://doi.org/10.1007/s00484-015-1014-x.
[49] V. Dervishi, C. Fleckenstein, M.A. Rahman, S. Pauleit, F. Ludwig, H. Pretzsch, T. Rötzer, Trees in planters – growth, structure and ecosystem services of Platanus x hispanica and Tilia cordata and their reaction to soil drought, Urban For. Urban Green. 86 (2023) 128024, https://doi.org/10.1016/j.ufug.2023.128024.
[50] J. Thierry, S. Herpin, L. Maturana, S. Demotes-Mainard, F. Rodriguez, P. Cannavo, P.-E. Bournet, Impact of a moderate water stress on the microclimatic services provided by street trees: an experimental study inside an outdoor canyon street scale model. Presented at the 35th Annual Congress of the International Association of Climatology, Toulouse, France, 2022.
[51] M.C. Peel, B.L. Finlayson, T.A. McMahon, Updated world map of the Köppen-Geiger climate classification, Hydrol. Earth Syst. Sci. 11 (2007) 1633–1644, https://doi.org/10.5194/hess-11-1633-2007.
[52] CAUE 77, Plantations d'arbres et changement climatique - 36e Arborencontre 2022, 2022 [WWW Document]. URL. (Accessed 10 December 2022).
[53] P. Cannavo, R. Guénon, G. Galopin, L. Vidal-Beaudet, Technosols made with various urban wastes showed contrasted performance for tree development during a 3-year experiment, Environ. Earth Sci. 77 (2018), https://doi.org/10.1007/s12665-018-7848-x.
[54] L. Vidal-Beaudet, C. Grosbellet, V. Forget-Caudel, S. Charpentier, Modelling long-term carbon dynamics in soils reconstituted with large quantities of organic matter, Eur. J. Soil Sci. 63 (2012) 787–797, https://doi.org/10.1111/j.1365-2389.2012.01494.x.
[55] USDA Natural Resources Conservation Service, n.d. Soil Texture Calculator [WWW Document]. URL https://www.nrcs.usda.gov/resources/education-and-teaching-materials/soil-texture-calculator.
[56] A. Bouthier, O. Scheurer, M. Seger, P. Lagacherie, N. Beaudoin, T. Deschamps, J. Sauter, J.-L. Fort, I. Cousin, Réservoir en eau du sol utilisable par les cultures, Editions ARVALIS, ARVALIS, 2022.
[57] D.K. Cassel, D.R. Nielsen, Field capacity and available water capacity, in: Methods of Soil Analysis: Part 1 Physical and Mineralogical Methods, Arnold Klute, 1986.
[58] FAO, R.G. Allen, L.S. Pereira, D. Raes, M. Smith, Crop Evapotranspiration (Guidelines for Computing Crop Water Requirements), FAO Irrigation and Drainage Paper, 2006.
[59] L. Chen, Z. Zhang, Z. Li, J. Tang, P. Caldwell, W. Zhang, Biophysical control of whole tree transpiration under an urban environment in Northern China, J. Hydrol. 402 (2011) 388–400, https://doi.org/10.1016/j.jhydrol.2011.03.034.
[60] J.B. Fisher, D.D. Baldocchi, L. Misson, T.E. Dawson, A.H. Goldstein, What the towers don't see at night: nocturnal sap flow in trees and shrubs at two AmeriFlux sites in California, Tree Physiol. 27 (2007) 597–610.
[61] C.M. Britton, J.D. Dodd, Relationships of photosynthetically active radiation and shortwave irradiance, Agric. Meteorol. 17 (1976) 1–7, https://doi.org/10.1016/0002-1571(76)90080-7.
[62] P. Bröde, D. Fiala, K. Błażejczyk, I. Holmér, G. Jendritzky, B. Kampmann, B. Tinz, G. Havenith, Deriving the operational procedure for the universal thermal climate index (UTCI), Int. J. Biometeorol. 56 (2012) 481–494, https://doi.org/10.1007/s00484-011-0454-1.
[63] D. Fiala, G. Havenith, P. Bröde, B. Kampmann, G. Jendritzky, UTCI-Fiala multi-node model of human heat transfer and temperature regulation, Int. J. Biometeorol. 56 (2012) 429–441, https://doi.org/10.1007/s00484-011-0424-7.
[64] D. Fiala, A. Psikuta, G. Jendritzky, S. Paulke, D.A. Nelson, W.D. van Marken Lichtenbelt, A.J.H. Frijns, Physiological modeling for technical, clinical and research applications, Front. Biosci.-Sch. 2 (2010) 939–968.
[65] G. Jendritzky, G. Havenith, R. de Dear, P. Weihs, E. Batchvarova, The Universal Thermal Climate Index (UTCI) for Assessing the Thermal Environment of the Human Being - COST Action 730 Executive Summary, 2009.
[66] J. Huang, J.G. Cedeño-Laurent, J.D. Spengler, CityComfort+: a simulation-based method for predicting mean radiant temperature in dense urban areas, Build. Environ. 80 (2014) 84–95, https://doi.org/10.1016/j.buildenv.2014.05.019.
[67] N. Bréda, H. Cochard, E. Dreyer, A. Granier, Field comparison of transpiration, stomatal conductance and vulnerability to cavitation of Quercus petraea and Quercus robur under water stress, Ann. For. Sci. 50 (1993) 571–582, https://doi.org/10.1051/forest:19930606.
[68] S. Demotes-Mainard, S. Herpin, A. Boukouya, S. Mballo, B. Dubuc, L. Ledroit, C. Le Lebras, D. Lemesle, P.E. Bournet, Impacts of the urban environment on well-watered tree architectural development and tree climate services. Presented at the 31st International Horticultural Congress, Angers, France, 2022.
[69] Q. Xiao, X. Fan, Y. Guo, S. Li, W. He, Y. Deng, Z. Xiao, P. Wang, C. Wu, Tree form characteristics as criteria for tree species selection to improve pedestrian thermal comfort in street canyons: case study of a humid subtropical city, Sustain. Cities Soc. 105 (2024) 105339, https://doi.org/10.1016/j.scs.2024.105339.
[70] S. Mballo, Quantification et modélisation des services climatiques rendus par les arbres dans une rue canyon, 2022.
[71] M. Liu, U. Pietzarka, M. Meyer, B. Kniesel, A. Roloff, Annual shoot length of temperate broadleaf species responses to drought, Urban For. Urban Green. 73 (2022), https://doi.org/10.1016/j.ufug.2022.127592.